

## Materials for Biomedical Applications

N. K. Vail<sup>1</sup>, L. D. Swain<sup>1</sup>, W. C. Fox<sup>1</sup>, T. B. Aufdemorte<sup>2</sup>, G. Lee<sup>3</sup>, and J. W. Barlow<sup>3</sup>

<sup>1</sup>BioMedical Enterprises, Inc  
Texas Research Park  
14785 Omicron Drive, Suite 205  
San Antonio, Texas 78245

<sup>2</sup>Department of Pathology  
The University of Texas Health Science Center at San Antonio  
San Antonio, Texas 78284

<sup>3</sup>Department of Chemical Engineering  
The University of Texas at Austin  
Austin, Texas 78712

### Abstract

This paper discusses two ceramic material systems for selective laser sintering (SLS) that are being developed for biomedical applications for use in repair of bone defects. SLS is the preferred method of fabricating ceramic implants that exhibit well defined porous microstructures. Implants fabricated in this manner have proven effective *in-vivo* showing excellent biocompatibility as well as considerable osseous integration and remodeling of the implant material. (**Keywords** : selective laser sintering, porous, ceramic implant, biocompatible)

### Introduction

Selective laser sintering (SLS) is one of the few rapid prototyping (RP) technologies that can fabricate complex objects from a wide variety of materials, including ceramics and metals. This makes SLS, and other capable processes, very attractive to manufacturers with needs for custom parts in novel materials. Historically, RP has been most accepted by large volume manufacturers requiring low volume prototypes in non-production and production materials. However, as RP has gained acceptance and evolved to offer greater accuracy and access to engineering materials, it has become attractive to low volume manufacturers who can benefit from fabrication in production materials.

The medical field is a specific example of low volume manufacturing. This area has seen limited use of RP, primarily as a means of guiding surgical procedures using tactile models derived from patient computed tomography (CT) data. In a classical RP application, James, *et al.*,<sup>1</sup> used stereolithography (SLA) models to plan the surgical correction of a facial defect. Others have utilized tooling capabilities of RP to provide solutions to specific patient defects. Holle *et al.*,<sup>2</sup> discuss the use of an SLA model to plan surgical shaping and attachment of autograft implants. Erickson, *et al.*,<sup>3</sup> cast custom titanium orbital implants. However, these latter two examples have notable drawbacks related to either multistep manufacturing processes or multistep surgical procedures. Direct fabrication of custom anatomical implants offers

streamlined manufacturing and provides a more simple surgical implementation. This paper discusses on going work to commercialize RP fabrication of custom anatomical implants for bone defect repair.

### Ceramic Implants

Repair of skeletal defects is limited to commodity devices, formable pastes, and surgically sculpted grafts. Custom anatomical implants show promise to provide improved osseous defect repair modalities. Such implants would be designed and optimized for a target defect using anatomical information and surgeon input, fabricated from an appropriate material exhibiting desired properties, and then implanted to effect repair and to restore form and function. 3D implant models would be derived with the aid of CAD and measurement data such as tactile, optical, or medical imaging techniques.<sup>4</sup> The combination of RP fabrication technologies and 3D implant models makes available for the first time the capability to fabricate custom anatomical implants from novel biocompatible materials. The ability to form strong, complex ceramic implants would alleviate existing problems with current materials and would open a new realm in osseous defect treatments.

In the present work, porous ceramic implants are fabricated using the established SLS based method illustrated in Figure 1.<sup>5,6</sup> This method uses conventional SLS technology to readily fabricate objects from polymer based materials. A substrate material, such as a ceramic powder, is combined with a polymeric binder that serves to bind the substrate particles during SLS processing into a contiguous object. The resulting “green” part is then subjected to post-processing techniques to thermally debind the green object and to impart strength to the bisque shape. The binder is combined with the substrate material by one of two methods: either simple mixing or encapsulation. Both methods have been used and offer distinct advantages in certain applications. However, the encapsulation method provides a clear advantage with respect to minimizing binder requirements, offering improved green part strength, and providing compositional control. Due to the porous nature of SLS parts, post-processing can include steps to introduce additional materials into the green part that serve to alter material composition as well as help to control part stability.

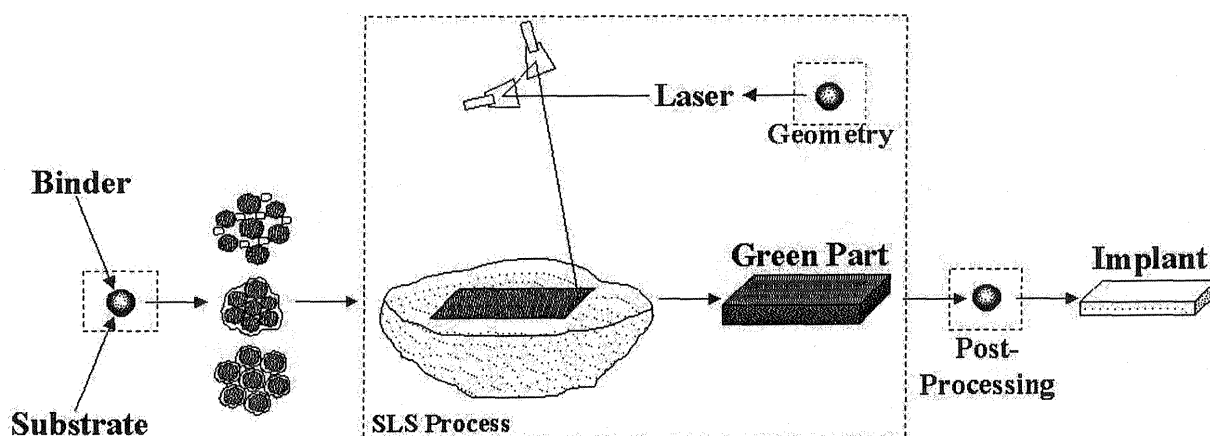


Figure 1. Fabrication of ceramic implants using indirect SLS technology.

### Calcium Phosphate Materials

Fabrication of calcium phosphate ceramic implants and preliminary biocompatibility results *in-vivo* have been discussed in previous work.<sup>7</sup> This benchtop process is currently being

commercialized to offer custom and commodity type implants as treatment modalities for bone defects resulting from trauma and disease. Present work is focused on materials formulation, implant properties quantification, and overall fabrication process control.

As noted above, SLS is used to create green ceramic implants. Feedstocks for SLS consist of polymer coated substrate ceramic particles. Current materials formulation uses fluidized bed coating, which yields discrete encapsulated particles with known polymer coating composition and is suitable for a broad range of particle sizes.

Two standard calcium phosphate substrate powder fractions, +45-63 $\mu$ m and +106-125 $\mu$ m, were encapsulated via fluidized bed processing using a latex based polymer.<sup>8</sup> Separate batches were prepared with different polymer contents in the range 10-40 vol. % (4-20 wt. %). Thermogravimetric analysis indicated polymer coating yields were greater than 90%. Particle size distribution analysis indicated the fluidized bed coating reduced the amount of fines present in the substrate material, probably either by material loss or by particle agglomeration (Figure 2). Agglomerated particles were prevalent in the smaller powder fraction as viewed by scanning

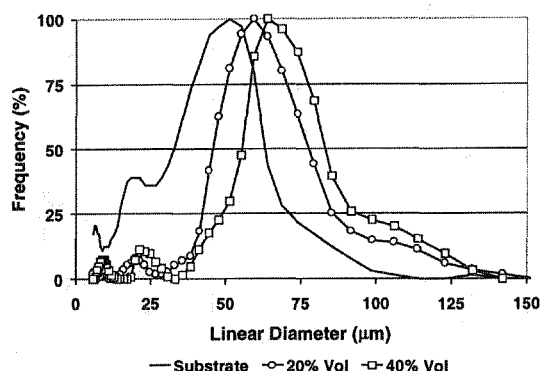


Figure 2. Particle size distributions for +45-63 $\mu$ m uncoated and coated calcium phosphate powders.

electron microscopy (SEM). The particle size distributions suggested the majority of particles are uniformly coated since the distribution forms changed little and are uniformly shifted to larger particle sizes with increased polymer coating. There was little broadening of the distribution, suggesting little agglomeration of larger particles and no occurrence of polymer fines due to coating inefficiencies or interparticle abrasion.

SLS processing conditions were determined with a +106-125 $\mu$ m powder containing 20 vol. % (8.7 wt. %) polymer coating. Two sets of three point bend specimens 1in. x 3in. x 0.25in. were fabricated in different orientations. The first set was oriented with the long specimen axis parallel to the laser fast axis and the second set was oriented with the long specimen axis perpendicular to the laser fast axis. Each set was fabricated using applied energy densities 0.5-3.0cal/cm<sup>2</sup>, where the applied energy density is defined as<sup>9</sup>

$$\frac{37.05P}{bs * scsp} [=] \frac{cal}{cm^2} \quad \text{Eq. 1}$$

with  $P$  the laser power in watts,  $bs$  the scan speed in inches per second, and  $scsp$  the scan vector spacing in mils. Green strength analysis showed a linear strength increase with increasing applied energy density. Maximum strength was about 200psi (1.4MPa), although no plateau or decrease in strength was observed over the parameter range. As expected, specimens scanned with the long axis perpendicular to the laser fast axis showed a steeper strength development than the other sample set. This phenomena has been shown to be a result of differences in the average temperature of the scanned area.<sup>5</sup>

SLS shrinkage factors were determined using three-point bend specimens ranging in size from 0.25in. x 1.0in. x 0.125in. to 1.0in. x 3.0in. x 0.25in. Two sets, oriented orthogonal, were fabricated using a constant applied energy density of 2.0cal/cm<sup>2</sup>. Figure 3 shows shrinkages in the x- and y-directions to be similar at about 0.5%. However, laser beam size compensation is

greater in the  $x$ -direction than in the  $y$ -direction (0.28mm vs. 0.15mm). The reason for this is not immediately clear, although the results are repeatable. Shrinkage and beam compensation do not vary significantly ( $p=0.01$ ) for similar specimens scanned with different applied energy densities. Verification of the process scaling parameters yielded parts with average nominal deviations of  $-0.06\pm 0.09$ mm, consistent with the material particle size.

In previous work, SLS green parts were post-processed using a sequence of infiltration, drying, and firing steps. Infiltrating solutions comprised of various compositions of calcium and phosphorous served to cement the particles and to alter the composition of the calcium phosphate material. Typical post-processing involved 3-4 infiltration steps to obtain a desired calcium phosphate composition, requiring 10-14 days of processing. In practice, implant delivery time is targeted for less than one week, and ideally 3-4 days once an implant design as been validated. Consequently, the post-processing has been refined and currently involves two infiltration/firing steps to obtain implants of a specific calcium phosphate composition and strength. To date, only the first infiltration step has been fully quantified.

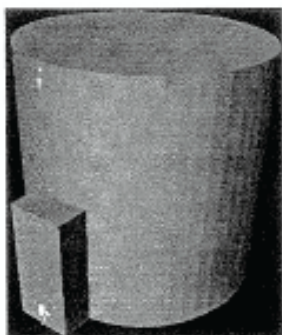


**Figure 4.** Compression test specimen. Dimensions: 0.3in. x 0.3in.

Cylindrical compression test specimens were fabricated via SLS using an optimal applied energy density of  $2.0\text{cal/cm}^2$  (Figure 4). These specimens incorporated measurement markers to reduce data acquisition variation. The green specimens had a compression strength of about 400psi (2.8MPa). Polymer content of the samples was determined thermogravimetrically to be 8.10 wt. % (18.6 vol. %).

Green test specimens were infiltrated with a 50/50 w/w aqueous methanol solution that contained 6-16wt. %  $\text{P}_2\text{O}_5$ . Liquid uptake analysis indicated the specimens had a porosity of  $48\pm 1\%$ . The infiltrated specimens were dried 8hrs at  $25^\circ\text{C}$  and 75% R.H. At this point, liquid mass loss was  $\sim 90\%$  of theoretical. The specimens were further dried at  $40^\circ\text{C}$  and 50% R.H. for two hours. Measured liquid loss was  $96.3\pm 0.2\%$  of theoretical.

The dried specimens were fired in air at  $800^\circ\text{C}$  for 1 hour. The heat ramp consisted of  $5^\circ\text{C}/\text{min}$  ramp to  $400^\circ\text{C}$  and a hold of 1 hour, followed by a  $2^\circ\text{C}/\text{min}$  ramp to the sintering temperature, followed by  $5^\circ\text{C}/\text{min}$  ramp to ambient temperature. Material balances indicated the mass change to be  $4.6\pm 2.5\%$  of theoretical.

Figures 5 and 6 show results for dimensional shrinkage and compressive strength, respectively. Shrinkage is anisotropic in the  $z$ -direction and typically twice the shrinkage in the  $xy$ -plane. Strength increases with increased solids in the infiltrating solution suggesting a dependence on the final part density. In addition to a density increase, the infiltrating solution alters the calcium phosphate composition, effectively lowering the CaO to  $\text{P}_2\text{O}_5$  ratio thereby reducing the melting point.<sup>10</sup> Localized melting point depression probably induces liquid phase sintering and increases shrinkage of the part. The median composition infiltrating solution (12 wt. %  $\text{P}_2\text{O}_5$ ) was chosen for the first infiltration step due to its moderate shrinkage and good

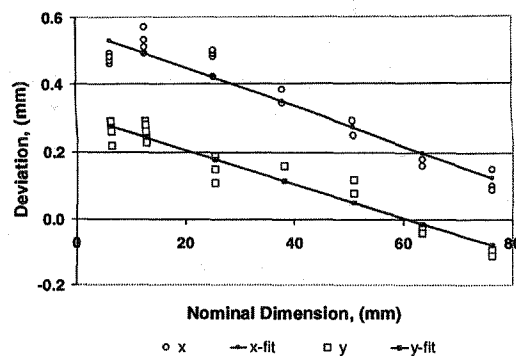


**Figure 3.** Shrinkage calibration for +106-125 $\mu\text{m}$  polymer coated calcium phosphate powder.

mechanical properties. These materials showed shrinkages of  $1.4 \pm 0.2\%$  in the *xy*-plane and  $2.7 \pm 0.4\%$  in the *z*-direction. Compressive strengths were  $5220 \pm 1090$ psi ( $36.0 \pm 7.5$ MPa) with a modulus of  $26000 \pm 6400$ psi ( $179.0 \pm 44.1$ MPa), suitable for low load applications.

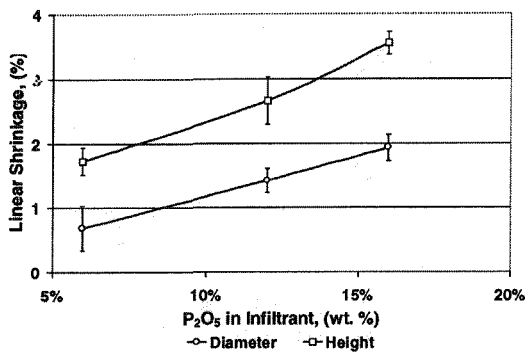


**Figure 5.** Shrinkage in the *xy*-plane and *z*-direction as a function of infiltrating solution composition for the first infiltration step in post-processing +106-125 $\mu$ m calcium phosphate SLS green parts. One hour at 800°C.

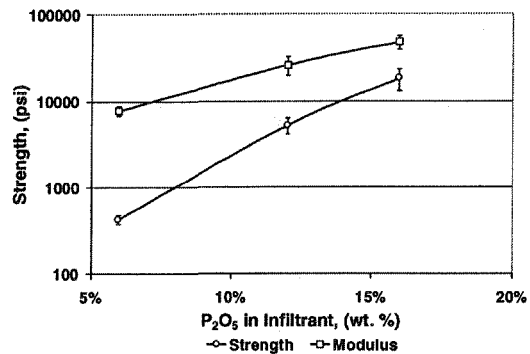


**Figure 6.** Strength and modulus as a function of infiltrating solution composition for the first infiltration step in post-processing +106-125 $\mu$ m calcium phosphate SLS green parts. One hour at 800°C.

Previous reports on this material system discussed the start of pre-clinical trials to assess the biocompatibility and efficacy of SLS formed calcium phosphate implants surgically placed in an alveolar ridge defect in canines.<sup>6</sup> Figure 7 shows the implant geometry used in these trials. Radiographic analysis showed the implants to be infiltrated with new bone (Figure 8). Some implant degradation was noted as changes in implant contour. The material showed a high degree of biocompatibility and mature mineralized bone was present throughout the implants, especially in the macropores (Figure 9).

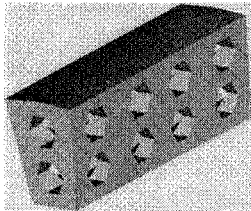


**Figure 7.** Implant model. Macropores are ~2mm in diameter. Dimensions: 3.3x6.6x15.3mm<sup>3</sup>.



**Figure 8.** Radiograph of SLS formed implant *in-vivo*, at three months. Bone fills the macropores and covers the implant.

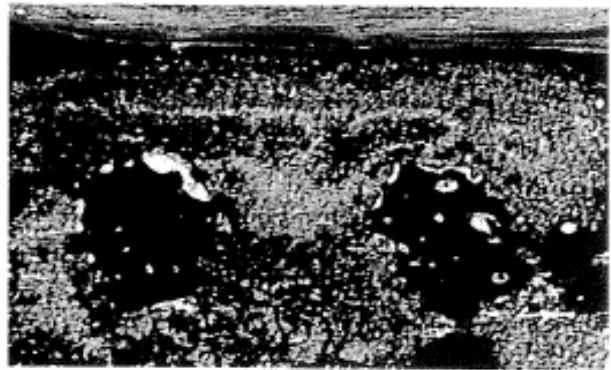


**Figure 9.** Histologic section showing new bone infiltration of macropores and microporous structure.

### Calcium Carbonate Materials

Natural calcium carbonate materials derived from marine corals have a history of use as osteoconductive scaffolds in bone defect repair.<sup>11</sup> These materials have two primary advantages in biomedical applications: 1) excellent biocompatibility, and 2) inherent microstructures very similar to natural bone (*i.e.* high porosity, well defined pore structures). Commercialized materials are either coarse granules or machined regular geometric shapes. Some materials have portions of the coral structure converted to hydroxyapatite. Machined shapes are brittle and, generally, are sculpted by the surgeon at the surgical site to fit the target defect. However,

failure to achieve close apposition to bone can lead to fibrous encapsulation and nonunion.<sup>12</sup> Hence, there is a need to examine alternative methods of forming site specific, strong coralline calcium carbonates that would facilitate their immediate use in osseous defect repair.

Coral (*pavona clavus*) was obtained in bulk from Tideline, Inc (Figure 10). Mercury intrusion porosimetry showed a narrow pore size distribution with a mean of about 100 $\mu$ m. The raw coral was broken into chunks, washed in a 5 wt. % Clorox solution followed by a water wash, then dried to constant weight. The cleaned material was crushed to powder and characterized by sieving. A single fraction +106-125 $\mu$ m was prepared. The mean particle diameter was 143.3 $\pm$ 35.5 $\mu$ m. X-ray diffraction (XRD) showed the coral to be aragonite, which, as confirmed by differential scanning calorimetry (DSC), is irreversibly converted to calcite on heating to 300°C. A powder sample was polymer encapsulated via fluidized bed coating. Thermogravimetric analysis indicated a polymer content of 4.34 wt. % (9.98 vol. %). Mechanical strength specimens (1in. x 3in. x 0.25in. and 0.3in. dia. x 0.3in.) were molded from the encapsulated powder. Three point bend analysis showed a modulus of rupture (MOR) of 179 $\pm$ 42 psi (1.2 $\pm$ 0.3MPa). Compressive strength analysis showed 225 $\pm$ 28psi (1.6 $\pm$ 0.2MPa). Molded specimens had a mean density of 1.32 $\pm$ 0.03 g/cm<sup>3</sup> or an equivalent porosity of 52% assuming a theoretical density of 2.75 g/cm<sup>3</sup> for the composite encapsulated material.

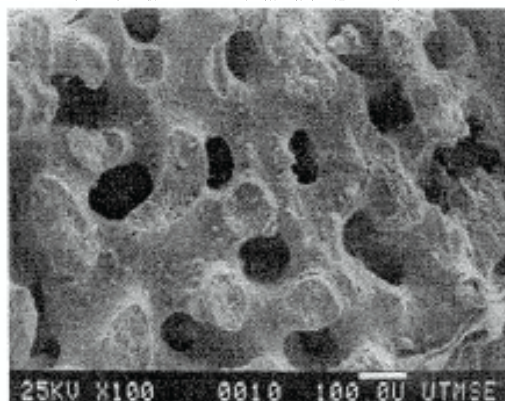
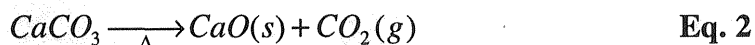


Figure 10. Microstructure of *pavona porites* coral at fracture surface.

To fabricate coralline calcium carbonate implants using the fabrication method of Figure 1, green parts must go through a post-processing step to remove the polymer binder and to impart strength. As with the calcium phosphate implants discussed above, infiltration is used to deposit material into the structure to control shrinkage and to bind the structure. However, the part must still go through a heat treatment cycle.

Calcium carbonate decomposes according to the following reaction:



Thermogravimetric analysis showed the conversion to calcium oxide becomes significant at about 600°C under normal atmospheric conditions. Therefore, it is possible to remove the polymer binder using typical debind procedures. However, sintering above 600°C in a controlled atmosphere may still be involved to achieve strong parts. Thermodynamic analysis of Eq. 2 shows the equilibrium CO<sub>2</sub> partial pressure approaches 1atm near 900°C.

Ultrafine precipitated calcium carbonate (PCC) was used as an infiltrating material (OMYA, Inc., Proctor, VT). This material is a concentrated aqueous slurry (76.4 wt. % solids) and has a median particle size of 0.48 $\pm$ 0.19 $\mu$ m. The slurry was diluted to 20 wt. % solids with 1 wt. % aqueous sodium dodecyl sulfate (Aldrich) and used to infiltrate molded compression test specimens. The specimens were saturated, weighed, and dried at ambient conditions. Comparison of porosity calculations of the infiltrated specimens to measurements of control specimens indicated complete saturation. There was no indication of PCC deposit on part surfaces.

Dried specimens were divided into three groups. The first group was tested immediately for compressive strength. The second group was subjected to a polymer debind step conducted in air at 450°C for 30 minutes. The specimens were weighed and tested for compressive strength. The last group was subjected to the same debind step as the second group but with a continuous CO<sub>2</sub> purge of 225cc/min. Following the 30 minute debind step, the samples were heated to 900°C at 5°C/min, held for two hours, then allowed to cool to room temperature. The specimens were weighed and tested for compressive strength.

Figure 11 shows the compressive strengths of all groups compared to the compressive strength of the initial green parts. The compressive strength of the infiltrated and dried specimens is about 2.5 times greater than the original green compressive strength. This probably reflects the part density increase of ~14%. The compressive strength is decreased more than a factor of three following the polymer debind step. This is as expected due both to loss of the actual system binder and to the subsequent decrease in density. However, it is most interesting to note the increase in strength of the parts following heat treatment at 900°C. There is a three fold increase in compressive strength that strongly suggests an increased physical interlocking of the calcium carbonate particle network. Median strength was 460±50psi (3.2±0.2Mpa), which compares favorably with reported strengths for commercial coral implants (626±350psi).<sup>13</sup> SEM clearly shows particle bridging, although the discrete calcium carbonate particles are still discernable (Figure 12). Grain coarsening is also evident, which suggests refinement of the heat treatment could improve mechanical strength. Porosity is still present and porosimetry indicated a median pore diameter of 30-40µm. XRD showed the parts to be pure calcite.

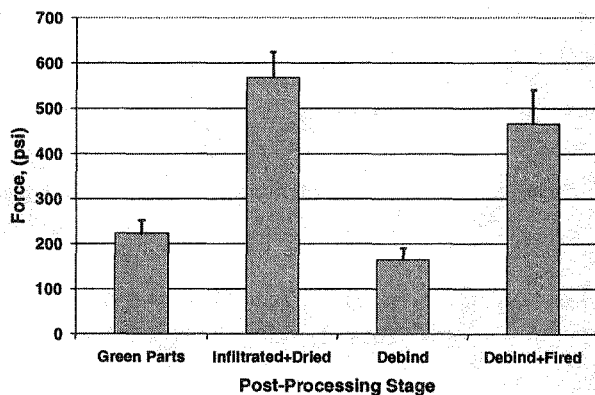


**Figure 11.** Comparison of compressive strengths of coralline calcium carbonate specimens at each step in the post-processing cycle.

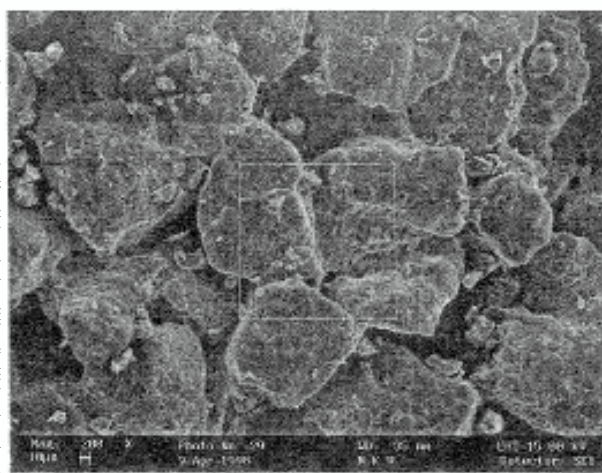


**Figure 12.** Fracture surface of completely post-processed coralline calcium carbonate part infiltrated with PCC

## Summary

Two ceramic material systems suitable for the fabrication of custom synthetic bone implants were presented. The first material system, comprised of calcium phosphate, has shown tremendous promise as an implant material. This material can be reproducibly processed to yield accurate parts with structures and strengths similar to natural bone. Work is continuing to refine the fabrication process and to more effectively control pore size of the final implant. Pre-clinical trials with SLS formed implants are very encouraging. Additional trials to demonstrate anatomical implants are planned precursory to clinical trials in humans.

The second material, comprised of coralline calcium carbonate, also shows promise as an implant material. Further work is required to refine the post-processing of this material to produce strong parts with controlled pore size. Pre-clinical trials to assess the biocompatibility and efficacy of SLS fabricated coralline calcium carbonate implants are planned.

### Acknowledgements

Portions of this work were supported under DoD STTR grants F41624-95-C-2008 and F41624-97-C-2000 and NIH SBIR grant 1-R43-DE-11749-01. The authors wish to thank Nicole Harlan of UT-Austin for assistance in preparing sintered calcium carbonate samples.

### References

---

- 1 James, W.J., M.A. Slabbekoorn, W.A. Edgin, and C.K. Hardin, "Correction of Congenital Malar Hypoplasia Using Stereolithography for Presurgical Planning," *J. Oral Maxillofac. Surg.*, **56**, 512-517, 1998.
- 2 Holle, J., K. Vinzenz, E. Würinger, K.-J. Kulenkampff, and M. Saidi, "The Prefabricated Combined Scapula Flap for Bony and Soft-Tissue Reconstruction in Maxillofacial Defects – A New Method", *Plastic and Reconstructive Surgery*, **98** [3], 542-552 (1996).
- 3 Erickson, D., Lt. Col., D.D.S., M.S., MacKown Dental Laboratory, Lackland Air Force Base, San Antonio, Texas, *personal communication*, 1997.
- 4 Vail, N.K., W. Wilke, H. Bieder, and G. Jünemann, in Marcus, H.L., *et al.* (Eds), "Interfacing reverse engineering data to rapid prototyping," in Marcus, *et al.* (Eds), *Solid Freeform Fabrication Symposium Proceedings*, **7**, 481-490, 1996.
- 5 Vail, N.K., Preparation and characterization of microencapsulated, finely divided ceramic materials for selective laser sintering, Ph.D. Dissertation, The University of Texas at Austin, 1994.
- 6 Balasubramanian, B., Study of the selective laser sintering of metal-polymer powders, Ph.D. Dissertation, The University of Texas at Austin, 1995.
- 7 Lee, G., W.C. Fox, T.B. Aufdemorte, and J.W. Barlow, "Biocompatibility of SLS-Formed Calcium Phosphate Implants", in Marcus, H.L., *et al.* (Eds), *Solid Freeform Fabrication Symposium Proceedings*, **7**, 15-21, 1996.
- 8 Vail, N.K., J.J. Beaman, D.L. Bourell, H.L. Marcus, and J.W. Barlow, "Development of a Poly(Methyl Methacrylate-co-n-Butyl Methacrylate) Copolymer Binder System," *J. Appl. Poly. Sci.*, **52**, 789-812, 1994.
- 9 Nelson, J.C., Selective Laser Sintering: A Definition of the Process and an Empirical Sintering Model, Ph.D. Dissertation, The University of Texas at Austin, 1992.
- 10 Faust, G.T., W.L. Hill, and D.S. Reynolds, "The Binary System  $P_2O_5$ - $2CaO \cdot P_2O_5$ ," *Am. J. of Sci.*, **242**, 447-477, 1944.
- 11 Papacharalambous, S. and K. Anastasoff, "Natural coral skeleton used as onlay graft for contour augmentation of the face," *Int. J. Oral Maxillo. Surg.*, **22**, 260-269, 1993.
- 12 Holmes, R. and H. Hagler, "Porous hydroxyapatite as a bone graft substitute," *J. Oral Maxillo. Surg.*, **45**, 421-429, 1987.
- 13 White, E. and E.C. Shors, "Biomaterial Aspects of Interpore-200 Porous Hydroxyapatite," *Dental Clinics of N. Am.*, **30**, 49-67, 1986.